MDPI

Article

Grid Turbulence Measurements with an Acoustic Doppler Current Profiler

Trygve K. Løken [1,*] , David Lande-Sudall [2], Atle Jensen [3] and Jean Rabault [4]

1   Division for Natural Sciences, Faculty of Education and Arts, Nord University, 8049 Bodø, Norway
2   Department of Mechanical Engineering and Maritime Studies, Faculty of Technology, Environmental and Social Sciences, Western Norway University of Applied Sciences, 5063 Bergen, Norway; david.lande-sudall@hvl.no
3   Department of Mathematics, Faculty of Mathematics and Natural Sciences, University of Oslo, 0851 Oslo, Norway; atlej@math.uio.no
4   Norwegian Meteorological Institute, 0371 Oslo, Norway; jean.rblt@gmail.com
*   Correspondence: trygve.loken@gmail.com; Tel.: +47-948-85-767

Abstract: The motivation for this study is to investigate the abilities and limitations of a Nortek Signature1000 acoustic Doppler current profiler (ADCP) regarding fine-scale turbulence measurements. Current profilers offer the advantage of gaining more coherent measurement data than available with point acoustic measurements, and it is desirable to exploit this property in laboratory and field applications. The ADCP was tested in a towing tank, where turbulence was generated from a grid towed under controlled conditions. Grid-induced turbulence is a well-studied phenomenon and a good approximation for isotropic turbulence. Several previous experiments are available for comparison and there are developed theories within the topic. In the present experiments, a Nortek Vectrino acoustic Doppler velocimeter (ADV), which is an established instrument for turbulence measurements, was applied to validate the ADCP. It was found that the mean flow measured with the ADCP was accurate within 4% of the ADV. The turbulent variance was reasonably well resolved by the ADCP when large grid bars were towed at a high speed, but largely overestimated for lower towing speed and smaller grid bars. The effective cutoff frequency and turbulent eddy size were characterized experimentally, which provides detailed guidelines for when the ADCP data can be trusted and will allow future experimentalists to decide a priori if the Nortek Signature can be used in their setup. We conclude that the ADCP is not suitable for resolving turbulent spectra in a small-scale grid-induced flow due to the intrinsic Doppler noise and the low spatial and temporal sample resolution relative to the turbulent scales.

Keywords: acoustic Doppler current profiler; grid-induced turbulence; turbulent spectra

1. Introduction

Due to their long profile range, autonomy and simple principals of operation, acoustic Doppler current profilers (ADCPs) are frequently used for turbulence measurements in the ocean and tidal channels [1–4]. As the technological advances keep improving the spatial and temporal resolution of the instruments, small-scale turbulence in the ocean, such as wake formation behind floating ice or human structures, may be studied with ADCPs. Some authors have also reported on turbulence measurements with ADCPs in laboratory facilities [5,6]. However, ADCPs have a measurement volume (~100 cm^3 when operated at the highest spatial resolution) that is typically much greater than the smallest eddy structures of the flow. Although the smallest structures cannot be resolved, some quantities such as the turbulent kinetic energy (TKE) primarily depend on the large energetic eddies and may therefore be estimated with ADCPs [6]. Due to its random nature, turbulence is usually described through statistical parameters like TKE, variance, TKE spectra and Reynolds stresses [7]. The parameters that can be reasonably well estimated are usually

first and second-order statistical properties because Doppler noise places a constraint on the accuracy of the instantaneous velocity estimates [8].

Various configurations with three to five beams are available for ADCPs [9]. A five beam broadband Nortek Signature1000 (kHz) ADCP was utilized in this study. The instrument has one vertical oriented beam $\mathbf{b_5}$ (instrument axis) and four slanted beams $\mathbf{b_1} - \mathbf{b_4}$ diverging at $\theta = 25°$ from the vertical and separated at $90°$ in the horizontal plane, i.e. in a Janus configuration. Five transducers emit acoustic waves along each beam, which are backscattered by particles suspended in the water. The particles are assumed to passively follow the fluid motion. The along-beam velocity component of the particles is calculated internally in the instrument from the Doppler shift of the reflected signal. Positive direction is defined radially away from the instrument and the beam velocities are denoted b_j for $j = 1, 2, ..., 5$. Each beam is divided into several cells that can be as small as 2 cm when the instrument is operated in the pulse-to-pulse coherent mode, also known as the high-resolution (HR) mode. Velocity profiles in three-dimensional space are therefore obtained, which increase the spatial distribution of data compared to traditional velocimeters, such as acoustic Doppler velocimeters (ADVs), that measure in a single point. This is a central motivation for trying to use ADCPs in laboratory applications. ADCPs perform non-intrusive measurements and the possibility of flow disturbance is practically non-existing over most of the profile, as long as the instrument axis $\mathbf{b_5}$ is perpendicular to the dominating flow direction, so that its wake does not pollute the measurement domain [7]. Another advantage of ADCPs is that they require no calibration, just occasional maintenance and operation checks [10].

However, ADCPs have limitations and sources of error that must be kept in mind when configuring the instruments and processing the data. Firstly, ambiguity errors are related to the aliasing of the Doppler signal. Acoustic velocimeters measure the phase shift ϕ of the backscattered signal, which lies in the range of $-180°$ to $180°$. If the particle velocity exceeds the velocity range associated with the instrument-specific ambiguity velocity U_{amb}, this will yield a corresponding phase shift outside the expected phase range, leading to ambiguity errors. The ambiguity velocity is defined as

$$U_{amb} = \frac{c}{8 F_0 \tau},\qquad(1)$$

where c is the speed of sound in water, F_0 is the sonar carrier frequency and τ is the time-lag between two consecutive pulses [4]. These errors can be identified as spurious data or large spikes in the time series and need to be corrected ("unwrapped") in the post processing. When the ADCP is operated in the HR mode, U_{amb} is quite low, so there is a trade-off between the cell size and velocity range (see, e.g., [11]). Secondly, acoustic instruments have intrinsic Doppler noise n in the beam velocity measurements, which is caused when the Doppler shift is estimated from finite-length pulses [12,13]. Doppler noise does not affect the mean velocity measurements (it is white noise), but influences the turbulence statistics by adding a positive bias to the highest frequencies in the TKE spectrum [14,15], which ultimately yields a higher measured TKE than the real TKE of the flow [16]. Thirdly, ringing and sidelobe interference may lead to errors close to the transducer and solid boundaries, respectively. Ringing is caused when the transducers continue to vibrate for a short time after the acoustic wave has been emitted, and the instrument cannot accurately record the backscattered signals until the transducer membranes have settled [6]. Among the three mentioned sources of error, the two former also apply for ADVs, while the latter is only relevant for ADCPs.

In many of the above-mentioned studies, ADV measurements are used as ground-truth values for comparison with ADCPs. Details on the operation of the instrument can be found in, e.g., [13,17]. ADVs are usually more accurate than ADCPs due to their small measurement volume (~1 cm^3), lower Doppler noise and higher temporal resolution. For example, ref. [13] found that an ADV was able to reproduce turbulence properties (Reynolds shear stresses) in a laboratory facility within 1% of a laser Doppler velocimeter.

However, the same study reported that the ADV measurements overestimated the velocity variance, especially in the stream-vise direction, due to Doppler noise. Whether caused by ambiguity, Doppler noise or any of the other sources, erroneous velocity measurements often occur as spikes in the time series, and various techniques have been proposed to mitigate the error of acoustic velocimeters, which often lead to overestimated root mean square (RMS) values and variance of the measured velocity [16]. For example, ref. [18] applied methods to remove erroneous spikes and to reduce Doppler noise from ADV data, which reduced the overestimated RMS velocities by up to 5% and 20%, respectively. The present study is an extension of the previous work where the ability of an ADCP to measure grid-generated turbulence properties is investigated and comparisons are made with a Nortek Vectrino ADV.

Grid-induced turbulence is a phenomenon that has been studied in wind tunnels [19–25], as well as in water tanks and flumes [26,27]. In wind tunnels and water flumes, the grid is fixed in space and the fluid flows past it. In water tanks, the grid and instruments are usually towed along the longitudinal direction of the tank, which puts a constraint on the duration of each repetition [26]. Most studies related to grid-induced turbulence focus on the decay of turbulent properties, such as velocity variance and TKE, as function of the normalized downstream distance to the grid x/M, where x is the downstream distance and M is the mesh size. For example, ref. [22] deduced a power law for TKE in the vertical direction TK_z, non-dimensionalized over the fluid speed U_f squared, $TK_z/U_f^2 = a(x/M)^m$, where $m \approx -1.3$ is independent of the fluid speed and a is a constant. Ref. [26] obtained the same power law and coefficient m in a water tank, where the towing speed U was the equivalent to the fluid speed.

In grid-induced turbulence, structures coexist over a range of spatial scales l, where $l = 2\pi/k$ and k is the turbulent wavenumber. The integral scale L corresponds to the largest turbulent eddies where TKE is produced, which are generated from grid-water interactions. Although the turbulence developing downstream of a grid is isotropic (directionally independent) and homogeneous (spatially independent) in theory, this is not obtained in reality at the integral scales [19]. As TKE cascades to the increasingly smaller structures, the flow is assumed locally isotropic and the TKE wavenumber spectra should be proportional to $k^{-5/3}$ according to the Kolmogorov law for developed turbulence [28]. This power law is valid in the inertial subrange that comprises scales l_{IS}, where $L \gg l_{IS} \gg l_K$ and l_K is the Kolmogorov microscale at which TKE is dissipated into heat due to viscosity. Since temporal measurements are made in this study, the turbulent wavenumber is related to the eddy frequency f through Taylor's hypothesis for steady state turbulence: $k = 2\pi f/\langle u \rangle$, where $\langle u \rangle$ is the time averaged velocity at which the flow is advected past the instruments. Hence, the frequency spectra should be proportional to $f^{-5/3}$ in the inertial subrange.

The aim of the present study is to investigate the ability of the Nortek Signature1000 ADCP, operated in the HR mode, to accurately resolve velocity variance and other TKE properties in fine-scale turbulence under well defined flow conditions. The turbulence was generated from a regular grid that was towed in a tank of quiescent fresh water. To our knowledge, turbulence from a towed grid has not yet been evaluated with an ADCP, hence this work is a new contribution to the literature. The paper is organized in the following manner. Section 2 describes the experimental facility and setup. The processing algorithms are given in Section 3 and the main findings of the study are presented and discussed in Section 4. Finally, the concluding remarks are summarized in Section 5.

2. Experimental Setup

The experiments were conducted in a 50 m long, 3 m wide and 2.2 m deep towing and wave tank in the MarinLab hydrodynamic laboratory at the Western Norway University of Applied Sciences. A coordinate system was defined with the (x, y, z)-axis to be aligned in the longitudinal, lateral and transverse (upward) directions of the tank, respectively, with $z = 0$ at the calm water surface. A computer-controlled carriage was towed along rails with a wire, and a second carriage could be coupled to the wire at any desirable distance behind

the main carriage. The grids were hanged from a mounting frame fixed to the front of the main carriage, which was manufactured from 100×50 mm sections EN 1.431 stainless steel, such that it was aligned with the yz-plane. Two regular square biplane grids were used; a large grid with mesh size $M = 0.25$ m and bar diameter $d = 5$ cm and a small grid with $M = 0.1$ m and $d = 2$ cm. The grids were manufactured from 6060 aluminium circular-section tubes. The tubes were welded into separate aluminium frames of 2.5 mm thickness, and tube ends left open to allow flooding of the grid. Both grids had a solidity coefficient $\beta = 2d/M - (d/M)^2 = 0.36$, which is similar to the grids used in, e.g., [21,27]. The grids were located in the tank center and spanned 1.4 m in width and 1.3 m in depth. Images and a schematic of the grid towing setup are shown in Figures 1 and 2, respectively.
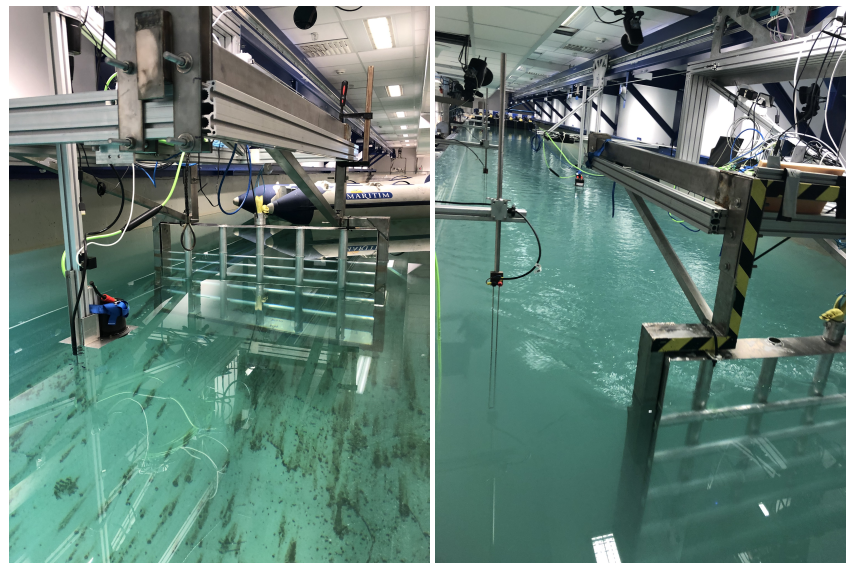
(**a**) Grid seen from downstream.   (**b**) Grid seen from upstream.

Figure 1. ADCP suspended from the main carriage during standstill (**a**) and from the second carriage during towing (**b**). Note that the grids are square, although they appear to be rectangular due to refraction at the water surface.

Safety concerns and practical limitations were taken into consideration in the process of designing the experimental setup. The towing carriage can provide a maximum horizontal total towing force of 6000 N and a maximum vertical load of 10,000 N. The outer frame of the turbulence grids was designed such that maximum stream-wise deflection would not exceed 3 mm at a towing speed of 2.5 m/s. In practice, with the turbulence grids mounted, the maximum towing speed tested for both grids was approximately 1.7 m/s. However, some carriage vibration were noted, possibly due to strong coherent vortex shedding from the outer frame, for speeds above 1.2 m/s and hence this study only considers towing velocities well below this region. Other practical considerations, which resulted in a limit to the outer grid dimensions were manual handling weight and limited ceiling height above the tank. Given that no crane was available, the grids were manufactured from hollow aluminum tubes, to keep handling weight under 40 kg. Similarly, the outer frame could not feasibly, nor safely, be installed if the frame dimensions exceeded those used.

The instruments were mounted at $x = 1.5, 2.5$ and 5 m behind the grid, either to the main carriage if $x < 2$ m or to the second carriage otherwise. The ADCP test matrix is listed in Table 1. The ADV test matrix was identical, except that the instrument was mounted at $x = 0.5, 2.5$ and 5 m behind the grid when the large grid was applied. Separate runs were performed with each instrument. The ADCP was mounted with the transducers submerged a couple of centimeters below the surface with the horizontal components of $\mathbf{b_1} - \mathbf{b_4}$ pointing in the $x, y, -x$ and $-y$- direction, respectively, and $\mathbf{b_5}$ pointing downwards. The ADV beams were aligned with the tank axes and the measurement volume was located

at $z = -0.5$ m. The carriage was accelerated at 0.5 m/s^2 until a constant towing speed of $U = 0.2$ or 0.4 m/s (also used in [26]) was reached, which yielded a mesh Reynolds number $Re_M = MU/\nu$ [23], where $\nu = 10^{-6}$ m^{2}s^{-1} is the kinematic viscosity of water, in the range 20,000–100,000. The mean and start/stop movement of the grid set up a seiche motion in the tank that was damped out after a couple of minutes. To ensure that the residual water motion was sufficiently damped out, new runs were initiated seven minutes after the carriage had been towed back to the starting position. A safety distance to the wave maker at the one end and the damping beach at the other end of the tank had to be maintained. Therefore, the total towing length was 31–34 m, depending on the distance between the grid and the instruments.
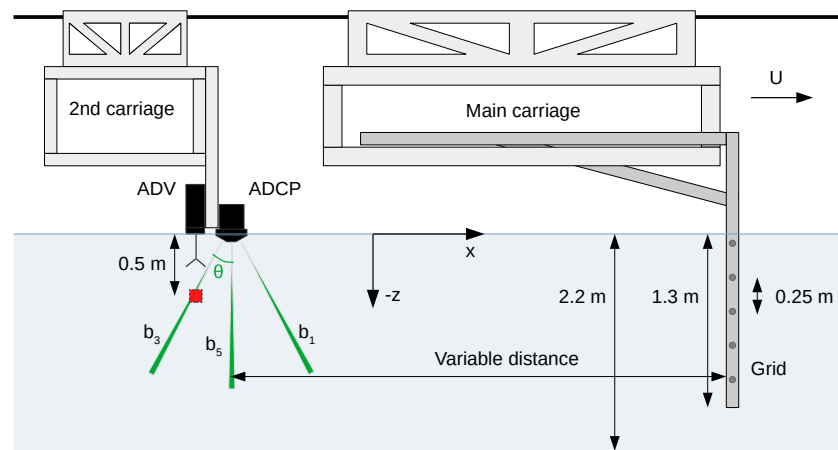

Figure 2. Schematics of the towing setup, here illustrated with the large grid. Both the ADCP and the ADV are illustrated (here mounted to the second carriage), but the two instruments were not deployed simultaneously. The red square indicates the position of the ADV measurement volume.

Table 1. Test matrix with the percentage of cells within b_5 that satisfied the ADCP quality criterion (beam correlation greater than 50%, more than 90% of the time).

x [m]	M = 0.25 m		M = 0.1 m	
	U = 0.2 m/s	U = 0.4 m/s	U = 0.2 m/s	U = 0.4 m/s
1.5	97	95	88	65
2.5	93	95	78	85
5	85	90	88	90

The ADCP range was set to 1.1 m on all beams, including a blanking distance (where no measurements were performed) of 0.1 m close to the instrument head in order to avoid transducer ringing. The beam correlation, which is a data quality indicator described in Section 3, was very sensitive to the instrument range, probably due to acoustic reflections in the tank. Several ranges were tested before adequate beam correlations were obtained. All the cells were located within the downstream grid area when the selected range was applied. Additionally, the ADCP beams did not reach the tank bottom and walls, hence sidelobe interference was avoided. The cell size was set to 2.5 and 5 cm for $U = 0.2$ and 0.4 m/s, which corresponded to 40 and 20 cells, respectively. The ADCP measurement volume was approximately 50–250 cm^3 ranging from the closest to the most distant cell with respect to the instrument, whereas the ADV measurement volume was around 1 cm^3. The sampling frequency was set to the maximum possible value of 8 and 200 Hz for the ADCP and ADV, respectively. The tank was seeded with 10 μm spherical glass particles, and almost 5 kg of seeding particles was necessary to obtain satisfactory backscattering. The seeding particles were well distributed in the tank after a couple of initial runs with the grid. The difference between no seeding and seeding can be seen in Figure 1a and Figure 1b, respectively.

3. Data Processing

From the raw data time series, data from the portion of the record that contained steady towing were carefully selected, i.e., data unaffected by acceleration and deceleration of the carriages. The rest of the time series was discarded. One run of steady towing lasted around 60–160 s, depending on the distance between the grid and the instruments and the towing speed, which means that the number of data points were in the order of 10^3 and 10^4 per run for the ADCP and the ADV, respectively. Due to the small amount of data points acquired with the ADCP, time series from several repetitions, typically two and four for towing speeds of 0.2 and 0.4 m/s, respectively, were concatenated to increase the number of independent data points. The 1/8 Hz = 0.125 s sampling interval was maintained between the last data point in the prior run and the first data point in the next run. Only time series from single ADV runs were used, as these contained much more data points. For the ADCP, some TKE frequency spectra were estimated from longer data point segments and they were almost identical to those estimated from shorter segments, which indicates convergence for second order statistical moments.

The concatenated time series were quality controlled by inspecting the beam correlation, which should exceed 50% for the ADCP and 70% for the ADV per manufacturer recommendations. Data points with lower correlation than the recommended values were flagged, and time series containing more than 10% low-correlation data were discarded. This was the case for some ADCP cells, typically far from the instrument transducer (an overview is given in Table 1 for $\mathbf{b_5}$), but all ADV time series contained satisfactory beam correlations. The ambiguity velocity U_{amb} was approximately 0.25 m/s for the ADCP, and ambiguity wrapping occurred in some situations in the longitudinally directed beams (b_1 and b_3). Data points that exceeded $\pm 7\sigma$ from the sample mean, where σ is the sample standard deviation, were identified as artifacts due to ambiguity wrapping and were unwrapped $\mp 2U_{amb}$ accordingly [4]. Figure 3 shows an example of ambiguity-wrapped raw data (blue points) which are corrected (red line).
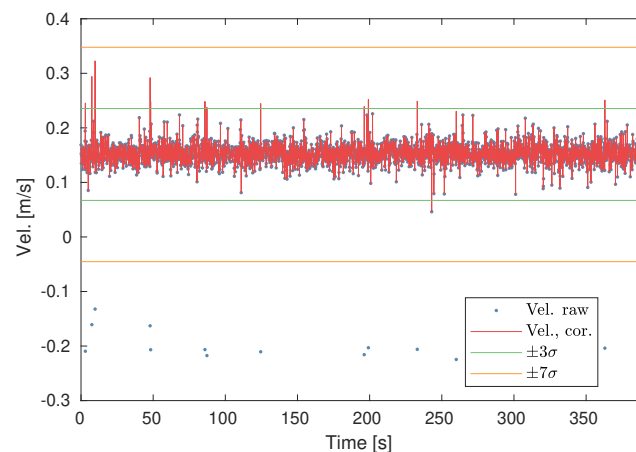

Figure 3. Quality control of a concatenated time series of steady towing at U = 0.4 m/s. Raw data are corrected for ambiguity wrapping when the velocity exceeds $\pm 7\sigma$. Spikes are identified when the corrected velocity exceeds $\pm 3\sigma$.

Some spikes occurred in the time series, resulting typically from unphysical data such as low correlation data, acoustic contamination specific to the laboratory or any of the other sources discussed in Section 1, but also from natural extreme values. Following [6], spikes were identified as data points that exceeded $\pm 3\sigma$ from the sample mean (indicated in Figure 3), which is similar to the minimum/maximum threshold filter described in [16]. In calculations of statistical parameters, such as variance, the spikes were discarded. However, in spectral analysis, continuous time series are required, so it is necessary to replace the discarded data with artificial data to obtain a statistically equivalent dataset to the real

dataset which would have been measured if there were no errors involved. Different approaches for replacement processes in the spectral analysis are reported in the literature. For example, ref. [29] interpolate neighboring data points in case of low correlation which may lead to spikes, and [6] include the spikes in the estimation of spectra. Both techniques will necessarily give some errors: due to the random nature of turbulence in the former case, especially if the turbulent scales are comparable to the sampling frequency, and the limited data quality in the latter case, particularly if there are solid boundaries in the vicinity of the instrument. In the present study, data points that exceeded $\pm 3\sigma$ from the sample mean were simply "cut" to $\pm 3\sigma$ from the sample mean, i.e. at the green lines in Figure 3. This strategy may reduce the effect of natural extreme values but the noise from unphysical data is mitigated. Some spectra were estimated with both strategies, and they were almost identical, except that the spectra from the "cut" time series were marginally less energetic, which may indicate that the noise level was reduced.

Statistical analysis was performed on the quality-controlled data. Although homogeneity between the instantaneous beam velocities was not obtained for the ADCP, homogeneity was assumed in the mean and the variance of the signal [1]. The mean longitudinal fluid velocity relative to the instrument $\langle u \rangle$, where the angled brackets denote time averaging over the whole time series, was obtained directly from the longitudinal component of the ADV and from

$$\langle u \rangle = \frac{\langle b_1 \rangle - \langle b_3 \rangle}{2 \cos \theta}, \tag{2}$$

of the ADCP [1]. The fluctuating velocity component in any direction $u_i' = u_i - \langle u_i \rangle$ was used in the turbulence analysis. Data that were flagged as spikes or with correlation less than the recommended values were discarded before calculating the velocity variance $\langle u_i'^2 \rangle$. The component of the TKE in the transverse (vertical) direction TK_z was defined as $TK_z = \langle w'^2 \rangle$. Since the transverse velocity was directly measured with the ADCP (b_5), no beam transformation was required to estimate TK_z. Following [9], the total TKE (denoted $q^2/2$ in their paper) TK was calculated as

$$TK_{ADV} = \frac{\langle u'^2 \rangle + \langle v'^2 \rangle + \langle w'^2 \rangle}{2}, \tag{3}$$

$$TK_{ADCP} = \frac{\langle b_1'^2 \rangle + \langle b_2'^2 \rangle + \langle b_3'^2 \rangle + \langle b_4'^2 \rangle - 2(2 \cos^2 \theta - \sin^2 \theta)\langle b_5'^2 \rangle}{4 \sin^2 \theta}, \tag{4}$$

for the ADV and the ADCP, respectively. Equation (4) combines the variance estimates from the ADCP transducers according to vector algebra to estimate the Cartesian 3D variance components given in Equation (3), with the assumption of homogeneity in variance over distances comparable to the horizontal separation of the bins [9].

Turbulent kinetic energy frequency spectra $PSD_w(f)$ were estimated from the transverse (vertical) fluctuating velocity component w' with the Welch method [30], which means fast Fourier transformation and ensemble averaging of overlapping segments. Each time series was divided into segments of 1024 data points with 50% overlap and a Hamming window was applied to each segment to reduce spectral leakage. The TKE frequency spectra represent the distribution of turbulent kinetic energy over the frequencies $0 < f < f_N$, where f_N is the Nyquist frequency, which was 4 and 100 Hz for the ADCP and the ADV, respectively. From Figure 3, it is clear that $u_i'/U \ll 1$, which indicates that the advection of turbulence past the instrument is dominated by the mean flow and not by the circulation of eddies, and that the assumption of Taylor's hypothesis is valid. Therefore, the TKE frequency spectra should be proportional to $f^{-5/3}$ in the inertial subrange.

Doppler noise often results in flat TKE frequency spectra, also known as the noise floor, towards the higher frequencies where the turbulent energy is low. From inspections of ADV data, it was observed that the noise floor was reached close to the Nyquist

frequency, and the noise floor was found by averaging the 20 highest frequencies of the TKE spectra, which corresponds to frequencies in the range 96–100 Hz. Following [31], the noise variance n^2 of the ADV was estimated by integrating the noise floor over the range of frequencies $0 < f < f_N$, assuming white noise spectra. The Doppler noise was removed from the ADV velocity variance statistically [32] by subtracting the noise variance, so that $\langle u_i'^2 \rangle = var(u_i') - n^2$. It was not clear whether the ADCP spectra, which are shown in Section 4, were obscured by noise. Hence, the turbulence properties obtained from the ADCP were not corrected for Doppler noise. Doppler noise is predominantly introduced in the horizontal velocity components in the case of ADVs, i.e., those ones perpendicular to the instrument axis [15,16]. Therefore, we mainly consider the velocity variance and spectra from the transverse (vertical) velocity component in this study.

4. Results and Discussion

The ADCP was able to reproduce the mean velocity in the longitudinal direction, as can be seen in Figure 4a. For the cells located at the same vertical level as the ADV measurement volume, the errors were less than 4%. Some missing cells were discarded because the beam correlation criterion stated in Section 3 (beam correlation must be greater than 50% more than 90% of the time) was not fulfilled. The measured velocities were about 10% lower than the towing speeds due to the grid-induced velocity deficit. The component of the TKE in the transverse direction TK_z, non-dimensionalized over the square of the towing speed U^2, is presented in Figure 4b. There was good agreement between the instruments for the high towing speed and the large grid, but the ADCP largely overestimated TK_z/U^2 in the other situations (by a factor of 2 for $U = 0.4$ m/s and approximately 5 for $U = 0.2$ m/s). A possible reason for this could be Doppler noise in the ADCP, which can cause a high bias in estimators related to TKE [1]. As stated in Section 3, estimated variance from the ADCP was not corrected for Doppler noise in the post processing. Figure 4 indicates reasonable homogeneity of the flow in the transverse (vertical) direction. Similar experiments with ADV measurements in the same tank with identical grids, reported homogeneous turbulence levels in the lateral direction within ±0.5%, with the exception of a local increase of ±2% behind the frame holding the grid [33].

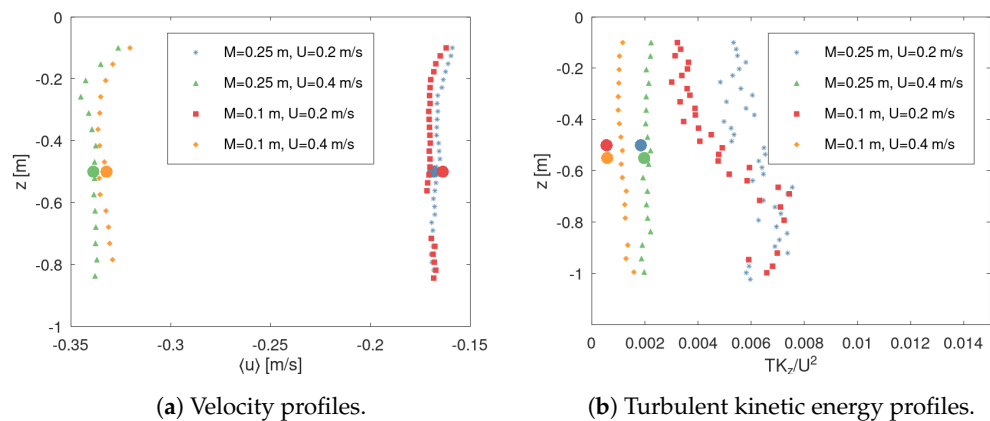(**a**) Velocity profiles.   (**b**) Turbulent kinetic energy profiles.

Figure 4. Vertical ADCP profiles at $x = 2.5$ m of (**a**) mean longitudinal velocity $\langle u \rangle$ and (**b**) TKE in the transverse (vertical) direction non-dimensionalized over the towing speed squared TK_z/U^2. The large dots are corresponding ADV data. Some of the ADV data points are slightly displaced in the vertical direction to increase the readability. Some data points are omitted due to low beam correlations.

Although the ADCP overestimated TK_z in the transverse (vertical) direction, this was not the case for the total turbulent kinetic energy TK estimated from Equations (3) and (4), presented in Figure 5. For the high towing speed, the values estimated from the ADCP were up to 35% smaller than the equivalent ADV values. The instruments agreed fairly well for the low towing speed, although these estimates were quite scattered in the vertical

profile. Doppler noise, which could vary between beams and cells, may have caused the deviations. Velocity components in all directions were used to estimate TK. It was observed from the ADV data that the grid-generated turbulence was not very isotropic. The ratio of $\langle w'^2 \rangle / \langle u'^2 \rangle$ was about 0.6, which is similar to the values obtained in another towing tank [26]. In comparison, grid-generated turbulence in a wind tunnel could reach a ratio closer to unity, for example, ref. [19] reported the ratio 0.8. Complete isotropy is not attainable in grid-generated turbulence due to the spatial inhomogeneity that arise from decay of TKE in the downstream direction [19].
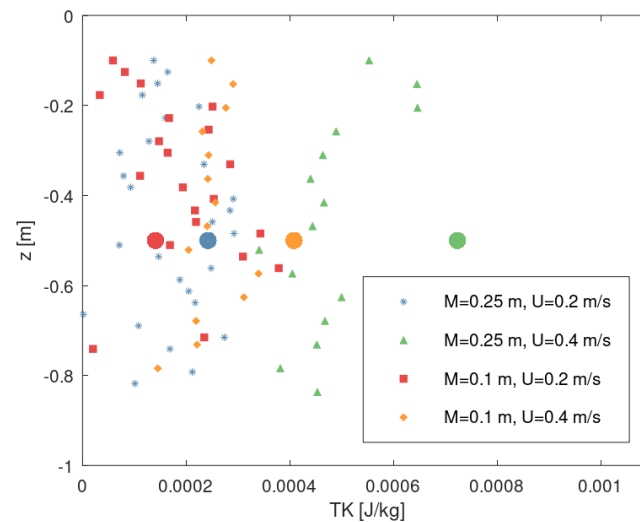

Figure 5. Vertical profiles of TK estimated from the ADCP and single values from the ADV (large dots) at x = 2.5 m. Some data points are omitted due to low beam correlations.

Figure 6 shows TK_z / U^2 versus downstream distance x/M for the large grid. The squares and triangles indicate the mean values obtained by ensemble averaging the ADCP cells located close to the ADV measurement volume in terms of depth. Typically, 11 cells were used to estimate the mean value, provided that all the time series satisfied the beam correlation criterion. A decay in TK_z can be observed, and the transverse components of the TKE decrease with increasing downstream distance approximately as $(x/M)^{-1.3}$, especially in the case of the ADV, which agrees with the findings of [22,26]. The ADCP data from the high towing speed approximately follow the same slope in the log-log plot, while the low towing speed data exhibit a weaker decay, which is in accordance with the mismatch observed between the ADV and the ADCP in TK_z / U^2 for the low towing speeds in Figure 4b. The low towing speed data also have large error bars for increasing downstream distance. The error bars represent the spread of the data obtained from the different cells and show two standard deviations of the sample of (11) cells. We do not attempt to justify the existence of a power law, as the data hardly span over one decade in distance, and only three data points are considered.

Turbulent kinetic energy spectra estimated from the transverse (vertical) fluctuating velocity components of the two instruments are presented in Figure 7. Spectra from the ADCP at 10 positions evenly distributed over the vertical profile are included, provided that the time series satisfied the beam correlation quality criterion. In general, it can be observed that the TKE level was higher with increasing towing speed and grid mesh size. The ADV spectra were proportional to the theoretical −5/3 power law over a wide range of frequencies, meaning that the instrument resolved the inertial subrange of turbulence. The ADV noise floor was reached well above 10 Hz and the noise level was approximately 10^{-8} m^{2}s^{-1}. However, the ADCP was not able to resolve the inertial subrange. The ADCP spectra appear to be quite flat around 10^{-4} m^{2}s^{-1}, which is consistent with the noise level of the Nortek Signature reported by [3] from tidal channel measurements.
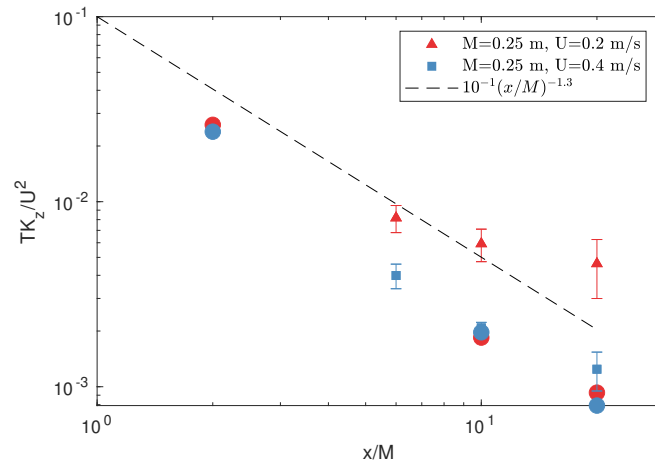
Figure 6. Decay of TK_z/U^2 as function of distance downstream of the grid for M = 0.25 m at different towing speeds (red: 0.2 m/s and blue: 0.4 m/s). ADCP cells (11 in most cases) are averaged to obtain the data points (triangles and squares) and the error bars show two standard deviations of the sample of cells. The large dots are corresponding ADV data.
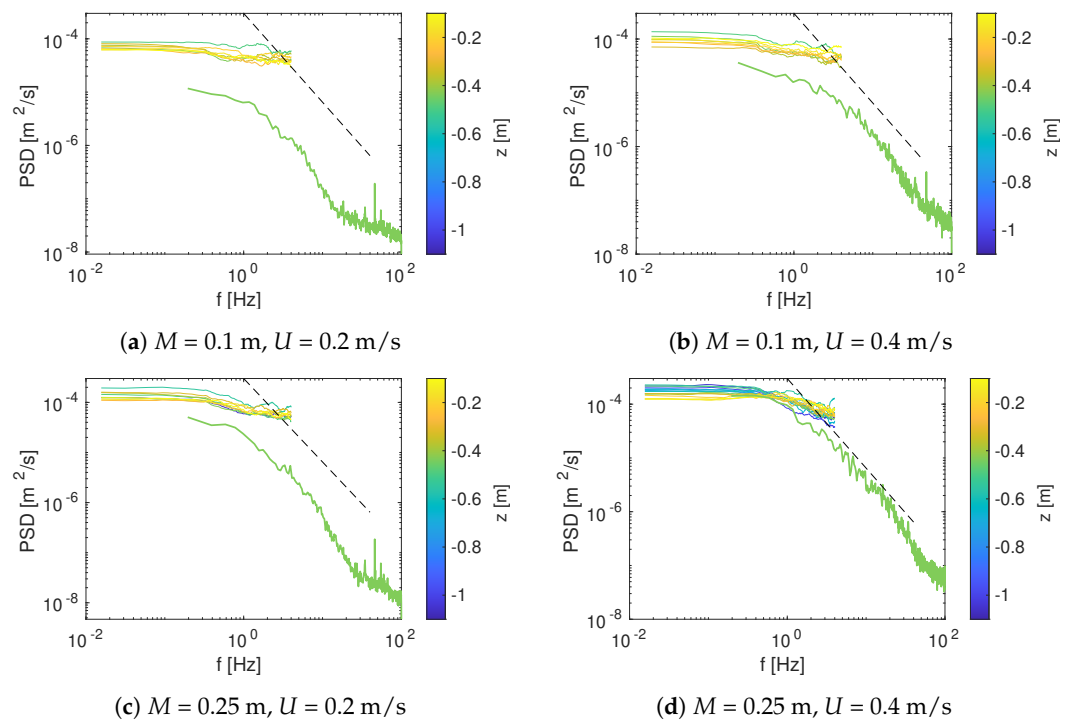

(**a**) M = 0.1 m, U = 0.2 m/s

(**b**) M = 0.1 m, U = 0.4 m/s

(**c**) M = 0.25 m, U = 0.2 m/s

(**d**) M = 0.25 m, U = 0.4 m/s

Figure 7. Turbulent kinetic energy spectra from the transverse (vertical) velocity component at x = 2.5 m, distributed over the vertical profile. The thick, green line is ADV data, and the dashed line is proportional to the theoretical $-5/3$ power law in the inertial subrange.

There are several possible explanations for the ADCP's failing ability to resolve the inertial subrange of turbulence. First, Doppler noise seems to prevent the instrument from detecting turbulent energy below approximately 10^{-4} m^{2}s^{-1}. This can be seen when the TKE starts to decrease with increasing frequency in accordance with the ADV spectra around 0.5 Hz, but then remain approximately constant. In other words, the TKE level at the scales associated with the inertial subrange in the flow may be too low to be detected by the instrument. On the other hand, it is not clear that the spectra flatten out in all situations. For example, in Figure 7d), the ADCP spectra decay with increasing frequencies until the Nyquist frequency of 4 Hz is reached, although with a smaller rate than the slope

of the ADV spectrum, which makes it difficult to conclude that the noise floor obscures the spectra.

Another possible explanation for the relatively flat spectra is the fact that the ADCP measurement volume is probably not adequately small to resolve the scales l_{IS} associated with the inertial subrange. In fact, water flume experiments on grid-generated turbulence suggest that the integral scale of turbulence in the longitudinal direction L_x is approximately $M/2$ at the downstream position $x/M \approx 20$ and slowly increasing with x/M [27]. The same findings are reported in the wind tunnel experiments of [21], who also found that the integral length scales L_y and L_z in the lateral and transverse directions, respectively, were about half the size of L_x. Assuming that the integral scale in the current experiments L was approximately equal to $M/2$, it is possible to make order of magnitude estimates of the TKE dissipation rate ϵ and the Reynolds numbers and eddy sizes at the various turbulent scales. Following [34], the TKE dissipation rate is estimated from the ADV data as $\epsilon = C_L(2TK_{ADV}/3)^{3/2}/L$, where $C_L = 0.5$ is a constant. The turbulence Reynolds number Re_L, which is the Reynolds number of the eddies within the integral scales, can be expressed as $Re_L = TK_{ADV}^2/(\epsilon\nu)$. In the inertial subrange, the eddies are associated with the Taylor microscale l_{IS} and the Taylor microscale Reynolds number Re_{IS}, which can be estimated as $l_{IS} = (10\nu TK_{ADV}/\epsilon)^{1/2}$ and $Re_{IS} = (20Re_L/3)^{1/2}$, respectively. In the dissipation range, the eddy size is associated with the Kolmogorov microcale l_K, which is determined by ϵ and ν through the relation $l_K = (\nu^3/\epsilon)^{1/4}$ [28].

The estimated TKE dissipation rates, Reynolds numbers and length scales summarized in Table 2, indicate that the turbulent eddies were on the order of 10 cm, 1 cm and 1 mm in the integral, inertial and dissipation range, respectively, for all reported combinations of grid size and towing speed. The ADCP cell size was 2.5 and 5 cm for $U = 0.2$ m/s and 0.4 m/s, respectively, which means that probably only the turbulent eddies in the integral scale were resolved by the instrument. However, the ADV measurement volume was approximately 1 cm^3, which suggests that the instrument was able to resolve turbulent eddies in the inertial subrange, according to Table 2. This is also confirmed in Figure 7, where the ADV spectra are proportional to the theoretical $-5/3$ slope over a wide range of frequencies. The Taylor microscale Reynolds numbers lie in the range of 120–290, which are typical values for fully developed grid-induced turbulence [24,25]. The turbulence Reynolds numbers are one order of magnitude smaller than the mesh Reynolds numbers.

Table 2. Turbulence statistical property estimates from ADV data at $x = 2.5$ m.

	M = 0.25 m		M = 0.1 m	
	U = 0.2 m/s	U = 0.4 m/s	U = 0.2 m/s	U = 0.4 m/s
$\epsilon \; [\mathrm{m^2 s^{-3}}]$	8.2×10^{-6}	4.2×10^{-5}	9.1×10^{-6}	4.5×10^{-5}
$L \; [\mathrm{m}]$	1.3×10^{-1}	1.3×10^{-1}	5.0×10^{-2}	5.0×10^{-2}
$Re_L \; [-]$	7.1×10^{3}	1.2×10^{4}	2.2×10^{3}	3.7×10^{3}
$l_{IS} \; [\mathrm{m}]$	1.7×10^{-2}	1.3×10^{-2}	1.2×10^{-2}	9.5×10^{-3}
$Re_{IS} \; [-]$	2.2×10^{2}	2.9×10^{2}	1.2×10^{2}	1.6×10^{2}
$l_K \; [\mathrm{m}]$	5.9×10^{-4}	3.9×10^{-4}	5.8×10^{-4}	3.9×10^{-4}

5. Conclusions

In this work, the ability of the Nortek Signature1000 five beam ADCP operated in high resolution mode to measure fine-scale turbulence was investigated. The provided experimental validation of the effective cutoff frequency and turbulent eddy size, indicates under which flow conditions the instrument can resolve turbulence. The research was carried out in a large towing tank where turbulence was generated from a towed grid. A Nortek Vectrino ADV was used as reference and the two instruments were in turn towed at a fixed distance behind the grid. Turbulence was described through the statistical parameters; variance, TKE and TKE spectra. The mean flow measured with the ADCP

was accurate within 4% of the ADV. Variance in the transverse (vertical) direction TK_z was reasonably well resolved by the ADCP when the large grid was applied with the high towing speed, but largely overestimated by a factor of 2–5 for the low towing speed and small grid compared with the ADV. This deviation was attributed to either Doppler noise, too small grid-generated eddies with respect to the sample volume/frequency or a combination of these. Better agreement was observed for total TKE, although the data were quite scattered along the vertical profile. A decay in TK_z was observed with increasing downstream distance to the grid approximately as $(x/M)^{-1.3}$, especially in the case of the ADV and the ADCP data from the high towing speed, which agrees with previous findings reported in the literature.

On the one hand, TKE and velocity variance are predominantly defined by the larger energetic eddies and were probably therefore reasonably well estimated by the ADCP in some grid size and towing speed combinations. On the other hand, spectra represent the distribution of TKE over a range of scales, and the minimum resolvable scale and frequency is limited by half the cell size and sampling frequency, respectively. Therefore, the ADCP was probably only able to measure the largest scales of the flow, and the inertial subrange was not visible in the spectra in the investigated flow. These assumptions are supported by provided estimates of the various turbulent length scales. Doppler noise may also have obscured smaller eddies around the Nyquist frequency. The spectral noise level of the Nortek Signature found in the towing tank was consistent with field experiments in tidal channels where the integral turbulent scales were much larger [3]. The present results indicate that the instrument is not suitable for grid turbulence measurements of this scale with regards to spectral properties. The largest turbulent scales should probably be at least an order of magnitude larger than the cell size to be able to resolve the inertial subrange, which may be difficult to obtain with grid generated turbulence in a laboratory.

Abbreviations

The following abbreviations are used in this manuscript:

ADCP	Acoustic Doppler current profiler
TKE	Turbulent kinetic energy
HR	High resolution
ADV	Acoustic Doppler velocimeter
RMS	Root mean square

References

1.　Stacey, M.T.; Monismith, S.G.; Burau, J.R. Measurements of Reynolds stress profiles in unstratified tidal flow. *J. Geophys. Res. Ocean.* **1999**, *104*, 10933–10949. [CrossRef]

2.　Guion, R.U.; Young, A.M. The frequency response of acoustic Doppler current profilers: Spatiotemporal response and implications for tidal turbine site assessment. In Proceedings of the 2014 Oceans-St. John's, St. John's, NL, Canada, 14–19 September 2014 ; IEEE: Piscataway, NJ, USA, 2014; pp. 1–10.

3.　Guerra, M.; Thomson, J. Turbulence measurements from five-beam acoustic Doppler current profilers. *J. Atmos. Ocean. Technol.* **2017**, *34*, 1267–1284. [CrossRef]

4.　Shcherbina, A.Y.; D'Asaro, E.A.; Nylund, S. Observing finescale oceanic velocity structure with an autonomous Nortek Acoustic Doppler Current Profiler. *J. Atmos. Ocean. Technol.* **2018**, *35*, 411–427. [CrossRef]

5.　Hardcastle, P. Investigation of estuarine turbulent flow and suspended sediment structures using high resolution coherent Doppler current profilers and a Sontek ADV Ocean Probe. In Proceedings of the Oceans' 97. MTS/IEEE Conference Proceedings, Halifax, NS, Canada, 6–9 October 1997; IEEE: Piscataway, NJ, USA, 1997; Volume 1, pp. 529–534.

6.　Nystrom, E.A.; Rehmann, C.R.; Oberg, K.A. Evaluation of mean velocity and turbulence measurements with ADCPs. *J. Hydraul. Eng.* **2007**, *133*, 1310–1318. [CrossRef]

7.　Nystrom, E.A.; Oberg, K.A.; Rehmann, C.R. Measurement of turbulence with acoustic doppler current profilers-sources of error and laboratory results. In Proceedings of the Hydraulic Measurements and Experimental Methods 2002, Estes Park, CO, USA, 28 July–1 August 2002; pp. 1–10.

8.　McMillan, J.M.; Hay, A.E.; Lueck, R.G.; Wolk, F. Rates of dissipation of turbulent kinetic energy in a high Reynolds number tidal channel. *J. Atmos. Ocean. Technol.* **2016**, *33*, 817–837. [CrossRef]

9.　Dewey, R.; Stringer, S. Reynolds stresses and turbulent kinetic energy estimates from various ADCP beam configurations: Theory. *J. Phys. Ocean.* **2007**, 1–35.. [CrossRef]

10.　Lipscomb, S.W. *Quality Assurance Plan for Discharge Measurements Using Broadband Acoustic Doppler Current Profilers*; Citeseer: Reston, VA, USA, 1995.

11.　Lhermitte, R.; Serafin, R. Pulse-to-pulse coherent Doppler sonar signal processing techniques. *J. Atmos. Ocean. Technol.* **1984**, *1*, 293–308. [CrossRef]

12.　Lohrmann, A.; Cabrera, R.; Karus, N. Acoustic Doppler velocimeter for laboratory use. In Proceedings of the Symposium on Fundamental and Advancements in Hydraulic Measurements, Buffalo, NY, USA, 1–5 August 1994; pp. 351–365.

13.　Voulgaris, G.; Trowbridge, J.H. Evaluation of the acoustic Doppler velocimeter (ADV) for turbulence measurements. *J. Atmos. Ocean. Technol.* **1998**, *15*, 272–289. [CrossRef]

14.　Dombroski, D.E.; Crimaldi, J.P. The accuracy of acoustic Doppler velocimetry measurements in turbulent boundary layer flows over a smooth bed. *Limnol. Oceanogr. Methods* **2007**, *5*, 23–33. [CrossRef]

15.　Khorsandi, B.; Mydlarski, L.; Gaskin, S. Noise in turbulence measurements using acoustic Doppler velocimetry. *J. Hydraul. Eng.* **2012**, *138*, 829–838. [CrossRef]

16.　Cea, L.; Puertas, J.; Pena, L. Velocity measurements on highly turbulent free surface flow using ADV. *Exp. Fluids* **2007**, *42*, 333–348. [CrossRef]

17.　McLelland, S.J.; Nicholas, A.P. A new method for evaluating errors in high-frequency ADV measurements. *Hydrol. Process.* **2000**, *14*, 351–366. [CrossRef]

18.　Doroudian, B.; Bagherimiyab, F.; Lemmin, U. Improving the accuracy of four-receiver acoustic Doppler velocimeter (ADV) measurements in turbulent boundary layer flows. *Limnol. Oceanogr. Methods* **2010**, *8*, 575–591. [CrossRef]

19.　Comte-Bellot, G.; Corrsin, S. The use of a contraction to improve the isotropy of grid-generated turbulence. *J. Fluid Mech.* **1966**, *25*, 657–682. [CrossRef]

20.　Uberoi, M.S.; Wallis, S. Effect of grid geometry on turbulence decay. *Phys. Fluids* **1967**, *10*, 1216–1224. [CrossRef]

21.　Comte-Bellot, G.; Corrsin, S. Simple Eulerian time correlation of full-and narrow-band velocity signals in grid-generated, isotropic turbulence. *J. Fluid Mech.* **1971**, *48*, 273–337. [CrossRef]

22.　Sirivat, A.; Warhaft, Z. The effect of a passive cross-stream temperature gradient on the evolution of temperature variance and heat flux in grid turbulence. *J. Fluid Mech.* **1983**, *128*, 323–346. [CrossRef]

23.　Raushan, P.K.; Singh, S.K.; Debnath, K. Grid generated turbulence under the rigid boundary influence. *J. Wind. Eng. Ind. Aerodyn.* **2018**, *182*, 252–261. [CrossRef]

24.　Gorbunova, A.; Balarac, G.; Bourgoin, M.; Canet, L.; Mordant, N.; Rossetto, V. Analysis of the dissipative range of the energy spectrum in grid turbulence and in direct numerical simulations. *Phys. Rev. Fluids* **2020**, *5*, 044604. [CrossRef]

25.　Kaminsky, J.; Birnir, B.; Bewley, G.P.; Sinhuber, M. Reynolds number dependence of the structure functions in homogeneous turbulence. *J. Nonlinear Sci.* **2020**, *30*, 1081–1114. [CrossRef]

26.　Liu, H.T. Energetics of grid turbulence in a stably stratified fluid. *J. Fluid Mech.* **1995**, *296*, 127–157. [CrossRef]

27.　Murzyn, F.; Bélorgey, M. Experimental investigation of the grid-generated turbulence features in a free surface flow. *Exp. Therm. Fluid Sci.* **2005**, *29*, 925–935. [CrossRef]

28.　Kolmogorov, A.N. The local structure of turbulence in incompressible viscous fluid for very large Reynolds numbers. *Dokl. Akad. Nauk. SSSR* **1941**, *30*, 301–305.

29. Zippel, S.F.; Thomson, J.; Farquharson, G. Turbulence from breaking surface waves at a river mouth. *J. Phys. Oceanogr.* **2018**, *48*, 435–453. [CrossRef]

30. Earle, M.D. Nondirectional and directional wave data analysis procedures. *NDBC Tech. Doc* **1996**, *96*, 780.

31. Thomson, J.; Polagye, B.; Durgesh, V.; Richmond, M.C. Measurements of turbulence at two tidal energy sites in Puget Sound, WA. *IEEE J. Ocean. Eng.* **2012**, *37*, 363–374. [CrossRef]

32. Lu, Y.; Lueck, R.G. Using a broadband ADCP in a tidal channel. Part II: Turbulence. *J. Atmos. Ocean. Technol.* **1999**, *16*, 1568–1579. [CrossRef]

33. Lande-Sudall, D.; Tolleifsen, S.; Gravelsæter, K.; Moen, H.; Bartl, J. Preliminary performance assessment from towing tank tests of a horizontal-axis turbine. In Proceedings of the 15th European Wave and Tidal Energy Conference (EWTEC 2023), Bilbao, Spain, 3–7 September 2023; Volume 15; pp. 5451–5458.

34. Variano, E.A.; Cowen, E.A. A random-jet-stirred turbulence tank. *J. Fluid Mech.* **2008**, *604*, 1–32. [CrossRef]